332 mechanical detwinning as a deformation mechanism in the β-metastable Ti-15Mo alloy during cyclic loading

Lola Lilensten, Fan Sun, Azziz Hocini, Guy Dirras, Philippe Vermaut, Frédéric Prima

{332}<113> mechanical detwinning as a deformation mechanism in the β-metastable Ti-15Mo alloy during cyclic loading

Lola Lilensten[1*], Fan Sun[1], Azziz Hocini[2], Guy Dirras[2], Philippe Vermaut[1,3], Frédéric Prima[1]

[1] : PSL University, Chimie ParisTech, CNRS, Institut de Recherche de Chimie Paris, Paris, France 75005

[2] : Université Sorbonne Paris Nord/Laboratoire des Sciences des Procédés et des Matériaux, CNRS-UPR 3407/99 avenue JB Clément, Villetaneuse, France

[3] : Sorbonne Universities, UPMC University Paris, UFR926, Paris, France 75006

* : Corresponding author : lola.lilensten@chimieparistech.psl.eu

Abstract

The cyclic shear study of the Ti-15Mo (wt.%) alloy, with twinning induced plasticity deformation mechanism, shows that whereas conventional {332}<113> twinning is obtained during forward loading, room temperature backward loading in Bauschinger tests are able to cause twins reversion, suggesting that detwinning can act as a proper deformation mechanism. After reversion, the mechanical twins leave behind residual bands with low misorientation (~2°) in the matrix, and secondary twins. When the backward deformation is continued, new twins of different {332}<113> systems favorable to backward stress are then produced in the microstructure. The formation of the various deformation products is rationalized by trace analysis and calculation of the resolved shear stress on the considered twinning systems.

Keywords

Ti-alloys, TWIP, detwinning, shear stress, mechanical twinning

Impact statement

Mechanical {332}<113> detwinning in a TWIP Ti-alloy is reported for the first time by performing Bauschinger shear tests.

Beta titanium alloys have long suffered from a lack of work-hardening rate, preventing them from a larger industrial development, in spite of attractive properties, such as corrosion resistance and low density. Combination of ductility and high strength, through a high work-hardening rate, was achieved thanks to the triggering of mechanical twinning, also called twinning induced plasticity (TWIP) effect. Alloys able to accommodate stress by this deformation mechanism belong to the family of β-metastable alloys, that also encompass alloys forming stress-induced martensite.

Interest and characterization of TWIP Ti-alloys focused, so far, mostly on uniaxial tests (tension or compression), for which the alloys display very promising mechanical properties, for a large range of deformation rates and temperatures [1–4]. Nevertheless, their behavior during more complex deformation pathways is still unknown. Among the remaining mechanical solicitation modes to investigate, to push forward the development of this alloys family, the cyclic behavior must be assessed.

Indeed, detwinning of mechanical twins upon load reversal has been evidenced in several materials such as face centered cubic coarse-grained TWIP steels [5,6] or hexagonal closed packed Mg (in which case, detwinning starts occurring during unloading) [7–9]. Regarding body centered cubic (bcc) structures, recent results on tungsten however showed that {112}<111> twins can form under room temperature and quasistatic strain rates in nanowires, but that their unstable nature leads to spontaneous detwinning during unloading [11,12]. This behavior was rationalized by the inclined twin boundaries with high interfacial energy, and seems to be specific, within the bcc family, to nanowires.

TWIP Ti-alloys, however, deform through the {332}<113> mechanical twinning system. In Ti-25Nb-25Ta alloy, {332}<113> twins formation was confirmed to occur by cyclic shear deformation, by analysis of the post-mortem microstructures [13]. Isolated {332}<113> twins were also reported in the microstructure of Ti-40Nb alloy deformed in fatigue at stresses below 225 MPa, followed by subsequent mechanical detwinning [14]. However, no detailed characterization was provided, and transformation of mechanical twins to stress induced martensite (the principal deformation mechanism) is suggested [14]. Detailed {332}<113> detwinning was only reported in Ti-Mo-Fe multilayered alloy and in Ti-Nb-Zr-O, where a thermal treatment following the deformation triggers the twin reversion [15,16]. For both alloys, the twin reversion starts from the intersection between the grain boundary and the twin tip, with a migration of the twin tip.

Facing these observations, the present study aims at unveiling the microstructural evolution in a TWIP Ti-alloy during load reversion. For that purpose, the behavior of the model Ti-15Mo TWIP alloy is investigated by Bauschinger tests. Detailed microstructural characterization of samples sheared only in forward loading and unloaded are compared to samples sheared in the forward direction, followed by a backward shear deformation.

Ti-15Mo (wt.%) alloy was prepared by arc-melting under high-purity Ar partial pressure. The initial pure metals were introduced in the chamber, and the ingot was melted 5 times to ensure chemical homogeneity. The ingots were then cut into slices that were subsequently cold-rolled with a thickness reduction of 80% to reach a final thickness of 1mm. 30mm-long (along the rolling direction) and 18-mm wide samples were cut out of the plates, recrystallized under vacuum at 1173K for 1.8ks, and finally water quenched, leading to a fully β microstructure. Both simple and Bauschinger shear tests were performed on a shearing device with a maximum load capacity of 100kN mounted on a MTS20 testing machine, details can be found in the supplementary material [17]. The mechanical behavior of the samples (30 x 18 x 1 mm^3 plates, effective sheared volume: 30 x 2 x 1 mm^3) was studied at a constant strain rate of $10^{-3}s^{-1}$ controlled by a video extensometer. Microstructural observations were performed in the central region of the sheared zone. Specimens were prepared by electropolishing with a $HClO_4$ – MeOH – butanol electrolyte. They were then analyzed on a Zeiss MERLIN scanning electron microscope (SEM) by a Brucker electron back-

scattered diffraction (EBSD) with step size 0.25µm or 0.083 µm and the data were processed with the OIM software. At last, transmission electron microscopy (TEM) was done. The sample was taken from the central region of the sheared zone as well and the shear direction was tracked on the TEM lamella by producing a straight edge. It was then thinned down manually and finally electropolished by a 4% perchloric acid solution in methanol, at -15°C, with the twinjet technique. The TEM observations were performed on a JEOL 2100 equipped with double-tilting holder.

Two types of shear tests are performed. In the first category, called “simple shear”, the samples are deformed (by applying a forward stress) until fracture, or until a set value, followed by unloading until the stress is back to zero, leaving a residual strain in the sample. The second category, entitled “Bauschinger”, follows the same initial deformation as in the “simple shear” mode, but after unloading, a backward stress is applied in the opposite direction of the forward stress until a set strain level. The Bauschinger tests are thus defined by their first level of forward strain (positive value), and their second one of backward strain (negative value).

The shear stress – shear strain curves, converted in equivalent stress and equivalent strain, are plotted together in Figure 1a. They are compared with uniaxial tensile curves acquired on dog-bone specimens of the same alloy. The plot shows a comparable behavior whether the sample undergoes a uniaxial or shear solicitation. Samples deformed in simple shear to 5 and 10%, and +5%/-2%, +5%/-5% and +10%/-2% Bauschinger samples are then studied in more details. The shear stress – shear strain curves are plotted in Figure 1b. One can notice that the two +5%/-2% and +10%/-2% Bauschinger tests end up, after unloading, at almost zero strain. A shear modulus of 29 +- 2 GPa is measured, and all the curves superimpose very well in the forward stress region. For better clarity, the three Bauschinger tests are also plotted in Figure 1c, where the backward segments are mirrored to positive stresses. The flow stress is monotonous, and upon unloading, some anelasticity is observed, similarly to previous observations in Ti-25Nb-25Ta alloy during cyclic shear [13], and also visible during the unloading stage of tensile experiments in TRIP-TWIP alloys [21]. This inelastic unloading is believed to be related, for the TWIP effect, to the backstress created by the geometrically necessary dislocations (GNDs) at the twin/matrix interfaces [22]. When a backward stress is applied (Bauschinger tests), a linear region appears on the shear curve, located at the beginning of the backward deformation, and is followed by a resumption of classical plastic deformation. The stress onset at the beginning of this linear part is around -75 MPa for all three tests. The work-hardening rate is plotted in Figure 1d and shows, in this region, a value of 5 GPa.

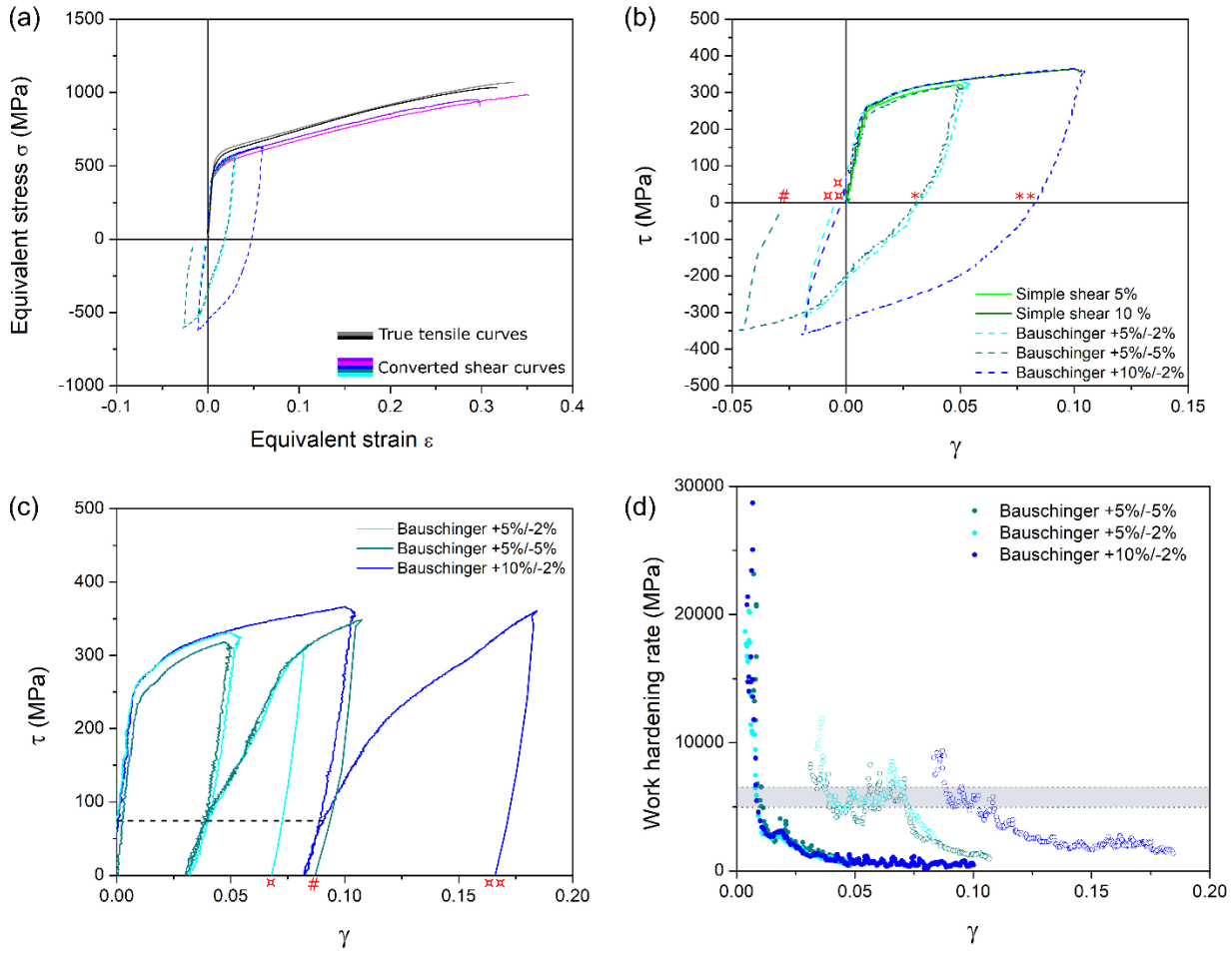

Figure 1: (a) Equivalent stress σ as a function of equivalent strain ε for Ti-15Mo tested in uniaxial tensile stress (black/grey curves) or by shear measurements (purple/pink curves : to fracture, blue/green curves : interrupted or Bauschinger tests). (b) and (c) Shear stress as a function of shear strain: simple shear and Bauschinger curves. The deformed states studied further by electron microscopy are indicated by red signs (and ** for 5 and 10% simple shear, and ¤, ¤¤ and # for +5%/-2%, +10%/-2% and +5%/-5% Bauschinger, respectively) (d) work-hardening rate of the Bauschinger curves in (c) (absolute values)*

Deformed microstructures of the five specimens where then characterized by EBSD. Figure 2 shows the inverse pole figures (IPF) maps and index quality (IQ) maps of the deformed microstructures. {332}<113> deformation twins are observed, and their boundaries are highlighted in red on the IQ maps.

One can see that for simple shear and unloading (* and ** states in Figure 1b), numerous twins are observed in the microstructures (Figures 2a-2b, and 2g-2h). The twinning density increases with deformation, with a total twin/matrix interface density of 0.175 μm^{-1} and 0.285 μm^{-1} for 5% and 10%, respectively. It is supposed that sample unloading does not allow twin reversion. Such hypothesis has been thoroughly made in studies of TWIP Ti-alloys deformed microstructures [18,19], and no {332}<113> detwinning was observed in situ in Ti-12Mo during unloading [20]. Similar assumption is therefore done in the present study.

After Bauschinger tests of +5%/-2% and +10%/-2% (¤ and ¤¤ states on Figure 1b and c), the sample has gone back to almost zero strain (see Figure 1b), through a backward stress deformation path

that includes a linear region (Figure 1c). Surprisingly, the resulting microstructures show a smaller number of deformation twins (Figure 2c and i). A decrease of the twin/matrix interface density is measured between the simple shear and the Bauschinger test, going from 0.175 μm^{-1} down to 0.066 μm^{-1} for +5% and +5%/-2%, respectively, and from 0.285 μm^{-1} down to 0.164 μm^{-1} for +10% and +10%/-2%, respectively. This suggests that some of the twins have been removed by the application of backward stress.

Finally, after +5%/-5% (# sign in Figure 1b and c), a high number of twins are found again, with an interface density of 0.295 μm^{-1}.

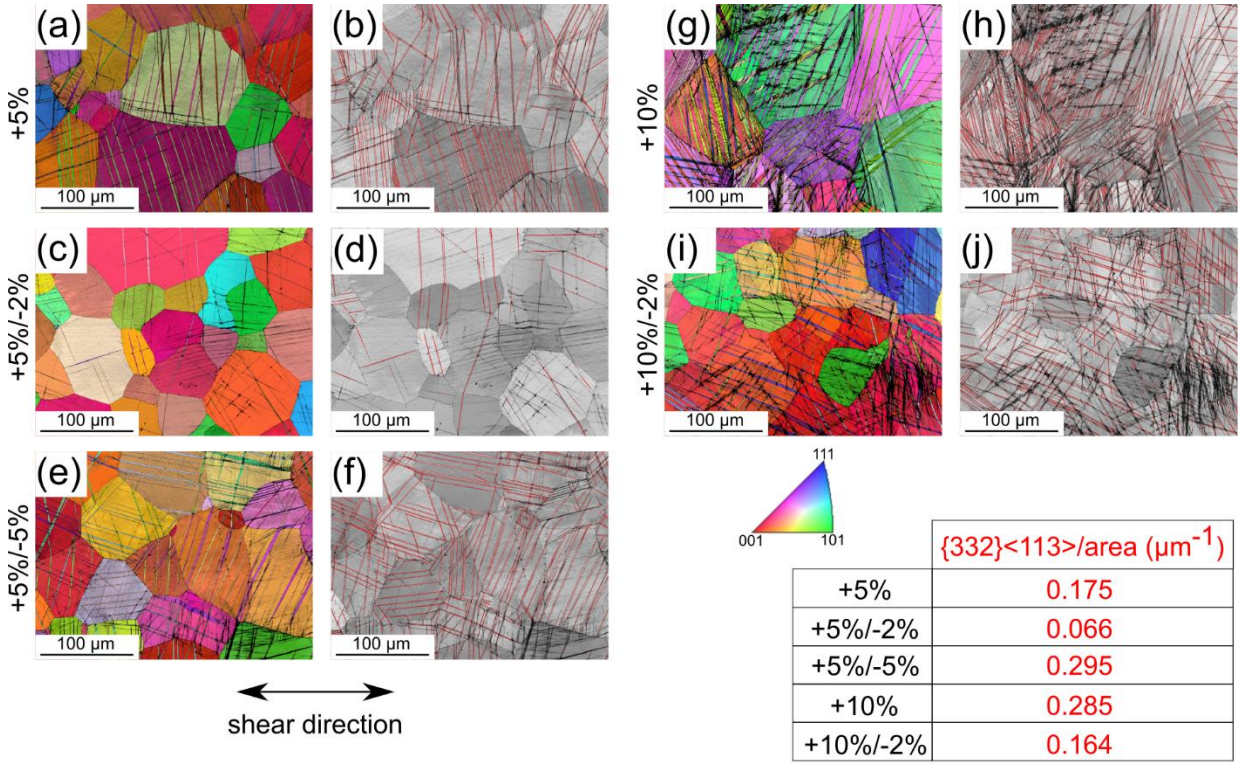

	{332}<113>/area (μm^{-1})
+5%	0.175
+5%/-2%	0.066
+5%/-5%	0.295
+10%	0.285
+10%/-2%	0.164

Figure 2 : IPF-EBSD maps ((a), (c), (e), (g), (i)) superimposed with the quality index of Ti-15Mo samples deformed in shear at 5% simple shear, +5%/-2% Bauschinger, +5%/-5% Bauschinger, 10% simple shear and +10%/-2% Bauschinger, respectively (step size: 0.25µm). The IQ maps of the EBSD maps are shown in (b), (d), (f), (h) and (j), with {332}<113> boundaries in red. The shear direction is horizontal and the IPF is plotted along the shear direction. The table provides the length of interface per surface, calculated over a total area of 450 x 300 µm².

Based on these results, it can be concluded that forward shear produces mechanical twins, which are not reversed upon simple loading but whose density drastically decreases when backward stress is subsequently applied to strain levels of -2%, and followed by unloading, which corresponds approximately to no residual strain. However, if the backward stress is continued to reach larger deformations, i.e. -5%, a large density of newly formed mechanical twins is observed. One must be careful to consider that these macro-scale findings aim at providing a trend. They depend on the resolution of the analyzing technique, here 0.25µm, and might therefore miss small scale features.

The twin reversion is likely to correspond to the linear segments of the shear curves during the backward section. It can then be considered as a deformation mechanism itself, as it does not happen spontaneously (unloading) and stress is required for activation. Based on the Bauschinger curves provided in Figure 1, it can be suggested that the triggering stress of detwinning is low, -75MPa, compared to the

260 ± 12 MPa yield strength of the forward segment, and that detwinning occurs simultaneously to the elasticity, leading to a high apparent shear modulus of about 5 GPa (see Figure 1d). This linear part is reduced for the +10%/-2% Bauschinger sample, suggesting a lower ability to detwin compared to the +5%/-2% or +5%/-5% samples. This is in good agreement with the larger amount of {332}<113> twin boundary length measured per unit area in the +10%/-2% (0.164 μm^{-1}) compared to the +5%/-2% sample (0.066 μm^{-1}) that has the same residual strain. This may be due to a complexification of the microstructure at larger strains, leading to a larger number of obstacles for detwinning.

In order to get a better insight on the twin reversion phenomenon, a closer look was taken at the +10%/-2% sample, which has a reduced length of interface per surface compared to the +10% sample, yet some remaining twins. Figure 3 shows a mapping with larger magnification and smaller step size of this sample, allowing to catch the details of the microstructure. On the Kernel average misorientation (KAM) map in Figure 3a, some strained bands are visualized, which also have lower IQ (Figure 3c). Some of them correspond to deformation twins (Figure 3b and Figure 3c), but some others do not, as the band in the black rectangle (plain line). Some strained bands are also found surrounding twins, such as the one observed in the dashed rectangle, as seen in Figure 3c. Plotting misorientation profiles along the blue lines 1 to 3, crossing the strained bands, reveal a small misorientation of 1 to 2° in these bands (Figure 3d). Finally, relevant {332} planes traces are provided in yellow on Figure 3c, showing that the strained bands are parallel to {332} planes. This suggests that the reversed twins leave behind residual strained bands slightly misoriented compared to the matrix, called “shadow-bands” in the following. The case illustrated in the dashed rectangle also shows that twin reversion can be complete or partial, with a residual twin remaining in the center of a shadow band. One can notice that such shadow-bands have not been observed in simple-sheared specimens, strengthening the hypothesis that no twin reversion occurs during unloading.

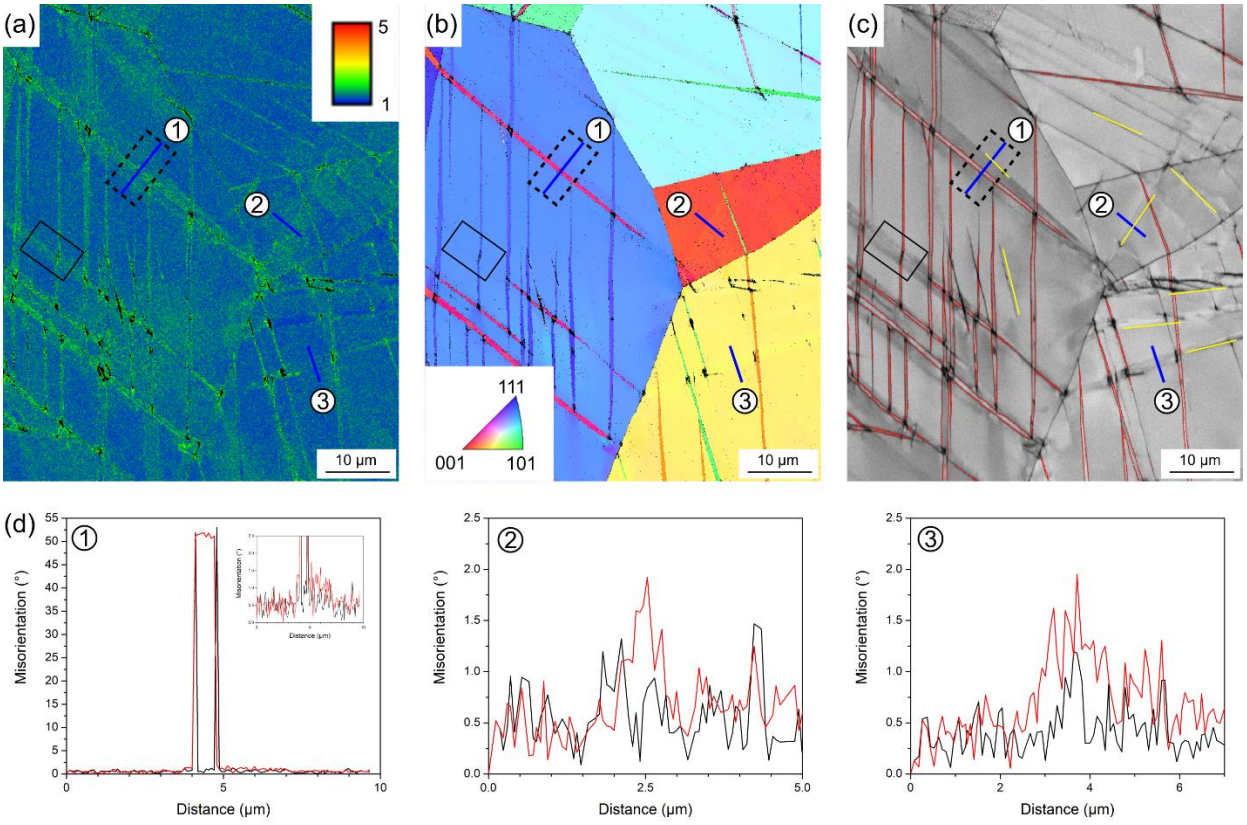

Figure 3: (a), (b) and (c) KAM map, IPF map and IQ with {332}<113> boundaries highlighted in red, respectively, of the sample deformed to +10%/-2% Bauschinger (step size: 0.083µm). (d) misorientation profiles along the blue (1) to (3). The black line shows the point-to-point misorientation and the red one the point-to-origin misorientation. The shear direction is horizontal and the IPF is plotted along the shear direction.

A closer-look to the microstructure of the +5%/-5% sample, provided in the Figure S1 of the supplementary material, shows that when the deformation is continued, new twins of different twinning systems are formed on top of the shadow-bands resulting from the detwinned former microstructure; and both coexist in the new microstructure.

TEM analysis was finally performed on the +5%/-2% sample to access the small-scale details of the reversed twins. The bright field image in Figure 4a shows the presence of several features in the β-matrix. Misorientation measurements and analysis of the orientation relationships (diffraction patterns in Figure 4b and pole figures of Figure 4c) allows to identify a “detwinned (DeT) band”, a residual {332}<113> twin and a secondary twin. The tilted image in Figure 4a and the DeT and matrix pole figures in Figure 4c measure a 1.7° misorientation between the DeT band and the matrix, in good agreement with the EBSD observations. The residual twin and the secondary twin are surrounded by large areas of DeT band. Formation of the DeT band seems to be the main twin reversion product, as it has been observed repeatedly on the macroscopical scale by EBSD.

To rationalize the formation sequence of the other observed features, orientation relationship between the matrix, the residual twin and the secondary twin are further studied, and *m* parameter, defined as a ratio measuring the resolved shear stress over the applied shear stress on the sample (details in

supplementary materials), is computed. This parameter can take values between -1 (unfavorable) and +1 (favorable) for a given twinning system.

The residual twin shows a direct {332}<113> twinning relationship with the matrix, with a *m* factor of 0.61 considering the forward shear direction. It is therefore suggested that this residual twin was a primary twin, formed during forward loading in the matrix. Its detwinning during backward loading results in the detwinned band. The boundary between the detwinned band and the matrix remains parallel to the residual twin boundary, suggesting that detwinning does not occur by migration of the twin tip, as observed during annealing [15,16], but rather by a mechanism leading to a thinning of the twin perpendicular to its {332} boundary planes.

The secondary twin does not have a have common {332} pole with the matrix (Figure 4c), but has one with the residual twin, with a corresponding *m* factor of 0.13 for backward loading. Although secondary twinning was often reported during simple uniaxial tensile experiments [19], the *m* factor computed for the forward stress in the present case would lead to a negative value of *m*, suggesting that this secondary twin originates from the primary twin during the backward deformation and is thus a second type of mechanism triggered upon backward loading, on top of detwinning, and called “backward secondary twinning”.

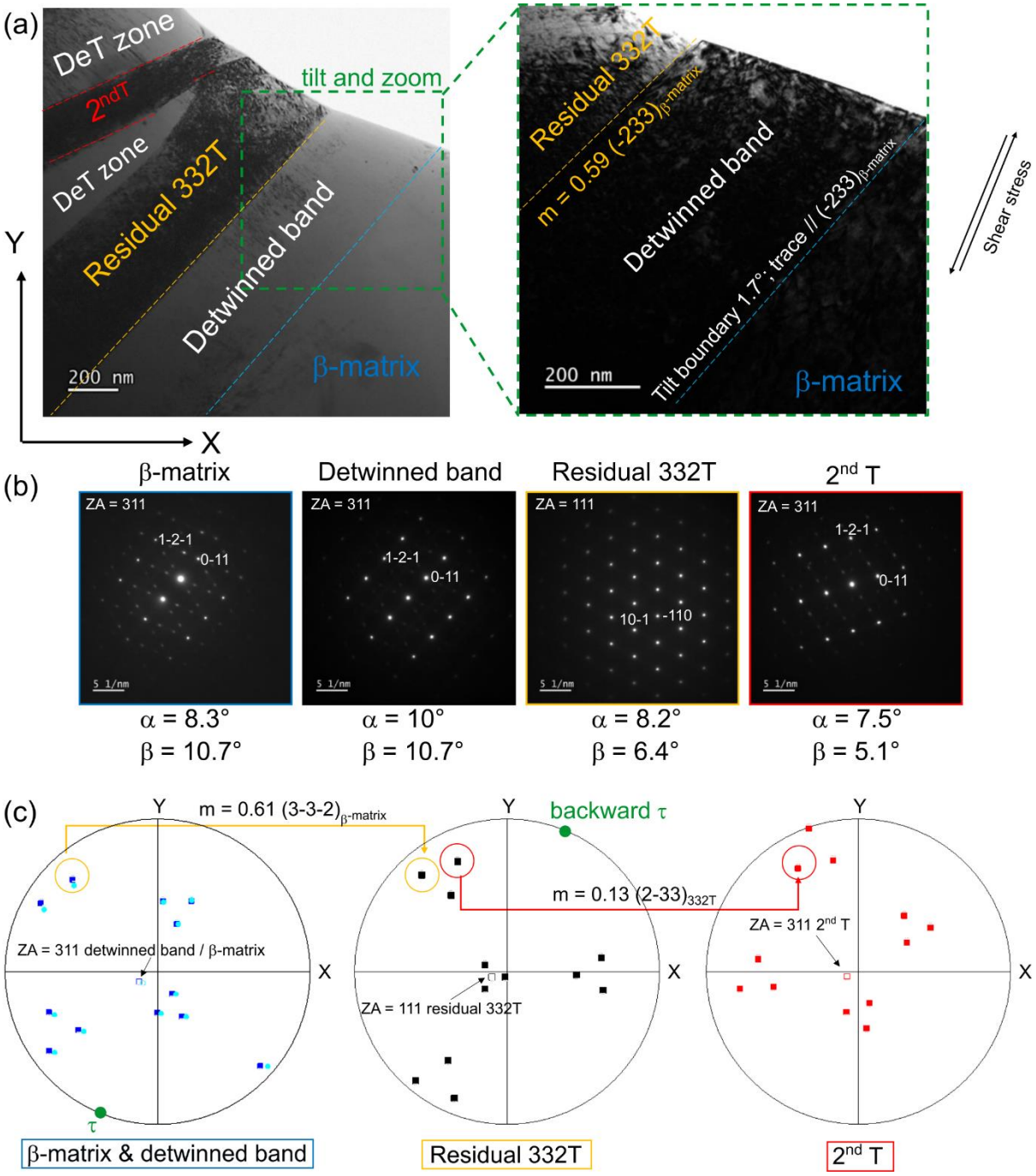

Figure 4: (a) bright field TEM image of the +5%/-2% Bauschinger sample and closeup (after tilting). (b) zone axis diffraction patterns for the four distinct features: β-matrix, detwinned band, residual 332T and 2nd twin. (c) Pole figures showing the {332} common poles for the matrix and the residual 332T, and for the residual 332T and the 2nd twin.

Overall, these results suggest that the {332}<113> twins forming during forward deformation, upon application of a backward stress, reverse by thinning down (along <332> directions), leading to detwinned bands with small misorientation, but can also produce backward secondary twins. The sum of these microstructural features – residual twins, detwinned bands and backward secondary twins – forms the

shadow-bands. The small scale of secondary and residual twins may explain that they are not always observed by EBSD.

In conclusion, a Bauschinger study in the TWIP Ti-15Mo (wt.%) alloy shows that mechanical {332}<113> twins formed by the forward stress deformation disappear upon applying a backward stress. The resulting microstructure, analyzed in detail by SEM and TEM, consists of shadow-bands, with small (~1-2°) misorientation with the matrix, that are the signature of twin reversion. Twin reversion appears to occur through a dual mechanism considering mostly the displacement of the {332} twin boundary plane, leaving behind detwinned zones displaying (332)-type planar interfaces with the native twin, but also the formation of backward secondary twins. At last, when the backward deformation is continued, new twins form in the microstructure. From these observations, we can conclude that {332}<113> mechanical twin reversion can be obtained, and that this may be considered as a deformation mechanism itself, as it contributes to the overall deformation of the alloy. Future work will be dedicated to rationalizing the detwinning mechanism, in order to provide better understanding of the nature of the defects in the detwinned bands, and to understand the detwinning critical stress.

Acknowledgements

LL thanks Inès Danard and Jérémy Da Conceiçao for the technical help.

Declaration of interest statement

References

[1] K. Yao, X. Min, S. Emura, K. Tsuchiya, Coupling effect of deformation mode and temperature on tensile properties in TWIP type Ti–Mo alloy, Mater. Sci. Eng. A. 766 (2019) 138363. https://doi.org/10.1016/j.msea.2019.138363.

[2] K. Yao, S. Xin, Y. Yang, Y. Du, J. Dai, T. Li, X. Min, Ultrahigh cryogenic strength and exceptional ductility at 20 K in a TWIP Ti–15Mo alloy, Scr. Mater. 213 (2022) 114595. https://doi.org/10.1016/j.scriptamat.2022.114595.

[3] K. Yao, X. Min, Abnormal strain rate strengthening and strain hardening with constitutive modeling in body-centered cubic {332}<113> TWIP titanium alloy, Acta Mater. 226 (2022) 117641. https://doi.org/10.1016/j.actamat.2022.117641.

[4] J.F. Xiao, Z.H. Nie, C.W. Tan, G. Zhou, R. Chen, M.R. Li, X.D. Yu, X.C. Zhao, S.X. Hui, W.J. Ye, Y.T. Lee, The dynamic response of the metastable β titanium alloy Ti-2Al-9.2Mo-2Fe at ambient temperature, Mater. Sci. Eng. A. 751 (2019) 191–200. https://doi.org/10.1016/j.msea.2019.02.068.

[5] C. D'Hondt, V. Doquet, J.P. Couzinié, Direct monitoring of twinning/detwinning in a TWIP steel under reversed cyclic loading, Mater. Sci. Eng. A. 814 (2021) 141250. https://doi.org/10.1016/j.msea.2021.141250.

[6] Q. Xie, J. Liang, A.D. Stoica, R. Li, P. Yang, Z. Zhao, J. Wang, H. Lan, R. Li, K. An, In-situ neutron diffraction study on the tension-compression fatigue behavior of a twinning induced plasticity steel, Scr. Mater. 137 (2017) 83–87. https://doi.org/10.1016/j.scriptamat.2017.04.041.

[7] L. Wu, S.R. Agnew, D.W. Brown, G.M. Stoica, B. Clausen, A. Jain, D.E. Fielden, P.K. Liaw, Internal stress relaxation and load redistribution during the twinning–detwinning-dominated cyclic deformation of a wrought magnesium alloy, ZK60A, Acta Mater. 56 (2008) 3699–3707. https://doi.org/10.1016/j.actamat.2008.04.006.

[8] S.M. Yin, H.J. Yang, S.X. Li, S.D. Wu, F. Yang, Cyclic deformation behavior of as-extruded Mg–3%Al–1%Zn, Scr. Mater. 58 (2008) 751–754. https://doi.org/10.1016/j.scriptamat.2007.12.020.

[9] S.-G. Hong, S.H. Park, C.S. Lee, Enhancing the fatigue property of rolled AZ31 magnesium alloy by controlling {10-12} twinning-detwinning characteristics, J. Mater. Res. 25 (2010) 784–792. https://doi.org/10.1557/JMR.2010.0094.

[10] L.M. Hsiung, D.H. Lassila, Shock-induced deformation twinning and omega transformation in tantalum and tantalum–tungsten alloys, Acta Mater. 48 (2000) 4851–4865. https://doi.org/10.1016/S1359-6454(00)00287-1.

[11] G. Sainath, S. Goyal, A. Nagesha, Plasticity through De-Twinning in Twinned BCC Nanowires, Crystals. 10 (2020). https://doi.org/10.3390/cryst10050366.

[12] X. Wang, J. Wang, Y. He, C. Wang, L. Zhong, S.X. Mao, Unstable twin in body-centered cubic tungsten nanocrystals, Nat. Commun. 11 (2020) 2497. https://doi.org/10.1038/s41467-020-16349-8.

[13] G. Dirras, D. Ueda, A. Hocini, D. Tingaud, K. Ameyama, Cyclic shear behavior of conventional and harmonic structure-designed Ti-25Nb-25Zr β-titanium alloy: Back-stress hardening and twinning inhibition, Scr. Mater. 138 (2017) 44–47. https://doi.org/10.1016/j.scriptamat.2017.05.033.

[14] A. Reck, S. Pilz, M. Kuczyk, A. Gebert, M. Zimmermann, Cyclic deformation characteristics of the metastable β-type Ti–40Nb alloy, Mater. Sci. Eng. A. 761 (2019) 137966. https://doi.org/10.1016/j.msea.2019.05.096.

[15] L. Qu, Y. Yang, Y.F. Lu, L. Feng, J.H. Ju, P. Ge, W. Zhou, D. Han, D.H. Ping, A detwinning process of {332}〈113〉 twins in beta titanium alloys, Scr. Mater. 69 (2013) 389–392. https://doi.org/10.1016/j.scriptamat.2013.05.028.

[16] I. Gutierrez-Urrutia, C.-L. Li, K. Tsuchiya, {332}<113> detwinning in a multilayered bcc-Ti–10Mo–Fe alloy, J. Mater. Sci. 52 (2017) 7858–7867. https://doi.org/10.1007/s10853-017-1032-7.

[17] S. Bouvier, H. Haddadi, P. Levée, C. Teodosiu, Simple shear tests: Experimental techniques and characterization of the plastic anisotropy of rolled sheets at large strains, J. Mater. Process. Technol. 172 (2006) 96–103. https://doi.org/10.1016/j.jmatprotec.2005.09.003.

[18] X. Min, X. Chen, S. Emura, K. Tsuchiya, Mechanism of twinning-induced plasticity in β-type Ti–15Mo alloy, Scr. Mater. 69 (2013) 393–396. https://doi.org/10.1016/j.scriptamat.2013.05.027.

[19] X. Zhou, X. a Min, S. Emura, K. Tsuchiya, Accommodative {332}〈113〉 primary and secondary twinning in a slightly deformed β-type Ti-Mo titanium alloy, Mater. Sci. Eng. A. 684 (2017) 456–465. https://doi.org/10.1016/j.msea.2016.12.025.

[20] B. Qian, L. Lilensten, J. Zhang, M. Yang, F. Sun, P. Vermaut, F. Prima, On the transformation pathways in TRIP/TWIP Ti–12Mo alloy, Mater. Sci. Eng. A. 822 (2021) 141672. https://doi.org/10.1016/j.msea.2021.141672.

[21] C. Brozek, F. Sun, P. Vermaut, Y. Millet, A. Lenain, D. Embury, P.J. Jacques, F. Prima, A β-titanium alloy with extra high strain-hardening rate: Design and mechanical properties, Scr. Mater. 114 (2016) 60–64. https://doi.org/10.1016/j.scriptamat.2015.11.020.

[22] O. Bouaziz, S. Allain, C. Scott, Effect of grain and twin boundaries on the hardening mechanisms of twinning-induced plasticity steels, Scr. Mater. 58 (2008) 484–487. https://doi.org/10.1016/j.scriptamat.2007.10.050.